



Femtosecond Third-Order Non-Linear Optical Properties of Unconstrained Green Fluorescence Protein Chromophores

Md Soif Ahmed¹, Chinmoy Biswas¹, Dipanjan Banerjee², Prabhakar Chetti³, Jye-Shane Yang⁴, Venugopal Rao Soma^{2*} and Sai Santosh Kumar Raavi^{1*}

¹Ultrafast Photo-Physics and Photonics Laboratory, Department of Physics, Indian Institute of Technology Hyderabad, Telangana, India, ²Advanced Centre of Research in High Energy Materials (ACRHEM), University of Hyderabad, Hyderabad, India, ³Department of Chemistry, National Institute of Technology, Kurukshetra, India, ⁴Department of Chemistry, National Taiwan University, Taipei, Taiwan

OPEN ACCESS

Edited by:

Gagan Kumar,
Indian Institute of Technology
Guwahati, India

Reviewed by:

Shashank Pandey,
Intel, United States
Bing Gu,
Southeast University, China

*Correspondence:

Venugopal Rao Soma
soma_venu@uohyd.ac.in
Sai Santosh Kumar Raavi
sskraavi@phy.iith.ac.in

Specialty section:

This article was submitted to
Optics and Photonics,
a section of the journal
Frontiers in Physics

Received: 06 April 2022

Accepted: 24 May 2022

Published: 04 July 2022

Citation:

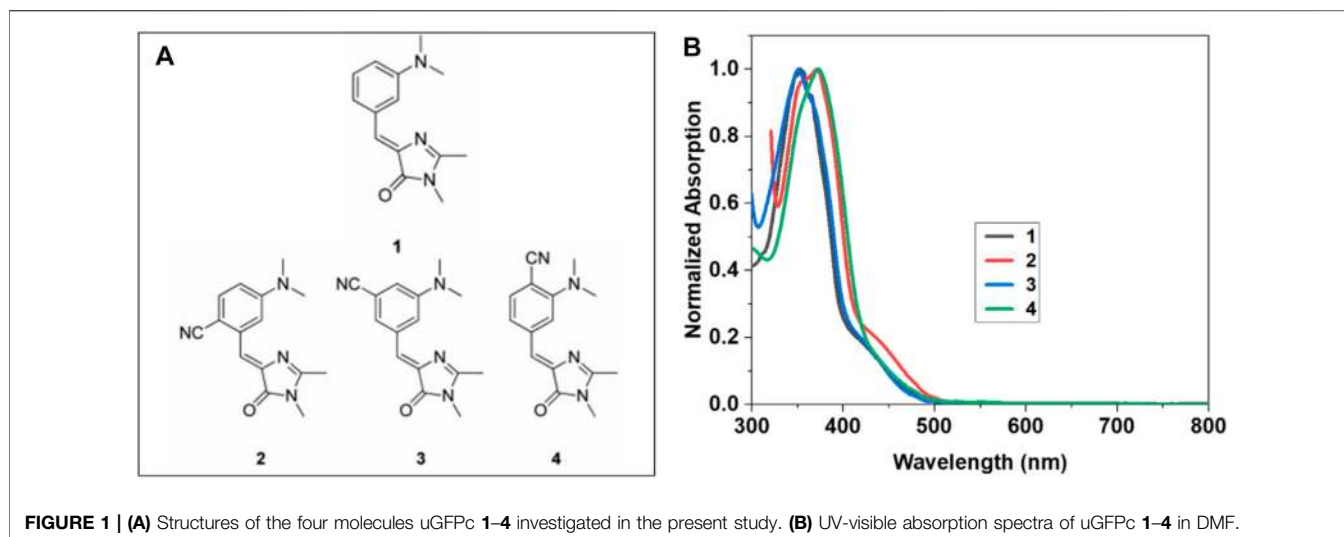
Ahmed MS, Biswas C, Banerjee D,
Chetti P, Yang J-S, Soma VR and
Raavi SSK (2022) Femtosecond Third-
Order Non-Linear Optical Properties of
Unconstrained Green Fluorescence
Protein Chromophores.
Front. Phys. 10:914135.
doi: 10.3389/fphy.2022.914135

We report herein results on the third-order non-linear optical (NLO) properties of four structurally unconstrained green fluorescence protein (GFP) chromophores, namely, **1**, **2**, **3**, and **4**. Using experimental techniques and theoretical calculations such as UV-visible spectroscopy, density functional theory (DFT), time-dependent density functional theory (TDDFT), and Z-scan techniques, we have investigated the linear absorption, ultrafast non-resonant third-order optical non-linearities, and the onset of optical-limiting thresholds of these benzylidenedimethylimidazolinone (BDI) dyes. The Z-scan measurements were performed at a wavelength of 800 nm with ~70 femtosecond (fs) pulses. We have witnessed a strong reverse saturable absorption (fitted to three-photon absorption) for all of the molecules with fs pulse excitation. The valley-peak curves obtained from the closed-aperture Z-scan technique revealed the positive non-linear refractive index (self-focusing) nature of these molecules. We have evaluated the various third-order NLO coefficients (second hyperpolarizability, $\gamma \sim 10^{-33}$ esu), which were found to be larger than those of similar molecules reported in the recent literature.

Keywords: green fluorescent protein, Z-scan technique, DFT, femtosecond, second hyperpolarizability, optical limiting

INTRODUCTION

Fluorescent proteins (FPs) have been omnipresent in biomedical research for the past decades because of their genetically encoded nature which enables researchers to covalently and uniquely label one specific protein with one specific color (1–3). In particular, succeeding the discovery of wild-type green fluorescent protein (WT-GFP) (4), WT-GFP and the subsequent GFP variants are readily cloned in other organisms. FPs have been recognized as an excellent two-photon absorber, which has been widely used in two-photon excitation fluorescence microscopy for their increased specimen penetration, reduced photo-toxicity, and negligible background fluorescence (5, 6). Even multi-photon fluorescence from these protein markers has been applied in the fields of cellular non-linear optical spectroscopy and microscopy. Thus, the non-linear optical (NLO) properties of the FPs have emerged to be very exciting in the photonics research world. The field of NLO deals with the interaction of applied intense laser light with various materials to produce new electromagnetic fields



changed in phase, frequency, or other physical properties (7–15). This field has received ample attention not only because of the several applications in dynamic holography, optical data storage, telecommunications, frequency mixing, etc. but also because of the fundamental sciences associated with polarization, charge transfer, conjugation, diradical character, etc. (16–19).

Besides their use in fluorescence imaging, FPs have been used for second-harmonic generation imaging. Second-harmonic imaging microscopy (SHIM) (20, 21) is a new NLO imaging technique where two photons at a fundamental frequency are converted into a single photon at the harmonic frequency. SHIM is correlative to the two-photon excitation fluorescence imaging method that is being used in microscopy to enhance the resolution (22). Recently, a few research articles have reported the second-order non-linear optical properties, particularly second-harmonic generation, and first hyperpolarizability values of green fluorescent proteins (1, 23, 24). However, there is a paucity of reports on third-order NLO responses of such kinds of GFP chromophores, although the GFP chromophores have been gradually characterized and become the subject of interest in cell imaging (25). In this article, we discuss the second hyperpolarizability values of four structurally unconstrained GFP chromophore analogs (uGFPc, **Figure 1A**) (26) associated with their third-order NLO properties. Tsai et al. (26) have reported that uGFPc have high fluorescence quantum yields, unlike the nearly non-fluorescent p-hydroxybenzylidenedimethylimidazolinone (p-HBDI) dye (a naturally occurring GFP chromophore). These uGFPc also differ from the structurally constrained analogs of p-HBDI, in which there exists covalent or non-covalent bridging of the two rings to instantaneously prevent the τ (C=C) and ϕ (C–C) torsions to reach a decent fluorescence recovery (27–29). Each of these molecules consists of an intense BDI-based locally excited $\pi - \pi^*$ transition band and a broad shoulder (absorbance up to 480 nm) attributable to the aniline-to-imidazolinone charge-transfer (CT) transition (**Figure 1B**) (30). Due to the presence of π -electron distribution in these molecules, strong non-linear optical (NLO) properties/coefficients are expected. To the best of our knowledge, no non-resonant measurements of uGFPc have been carried out to

date. Herein, we have carried out third-order NLO measurements of the four uGFPc, namely, **1**, **2**, **3**, and **4**, employing the Z-scan technique and estimated the values of $\chi^{(3)}$. We have observed that each molecule is showing three-photon absorption when we measured the open-aperture Z-scan study. We have also obtained the values of second hyperpolarizability (γ) from the Z-scan experimental data and the DFT/TDDFT calculations. The γ values of all of these molecules are effectively large.

EXPERIMENTAL DETAILS

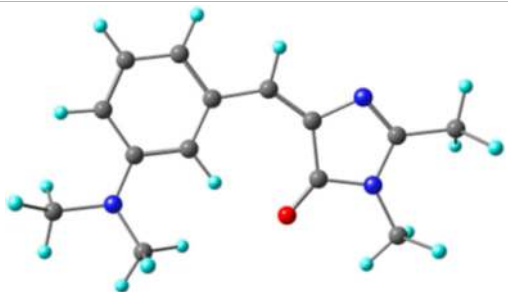
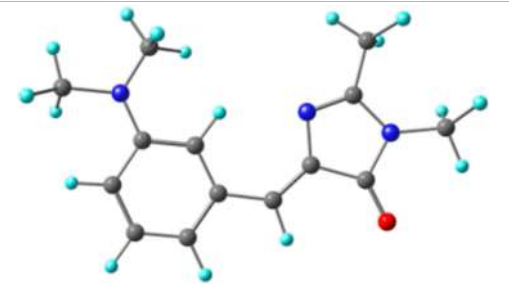
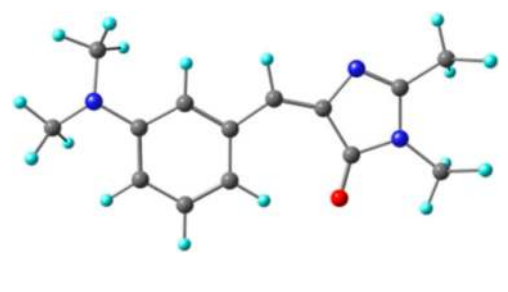
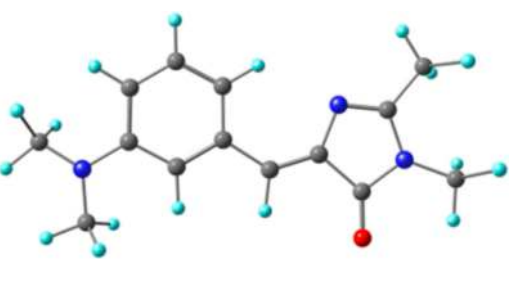
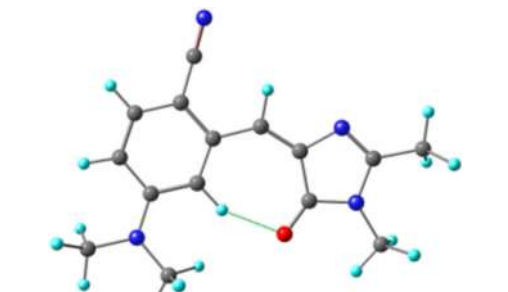
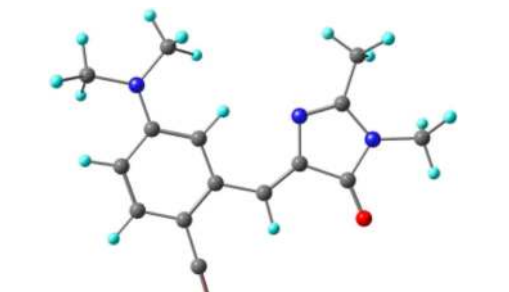
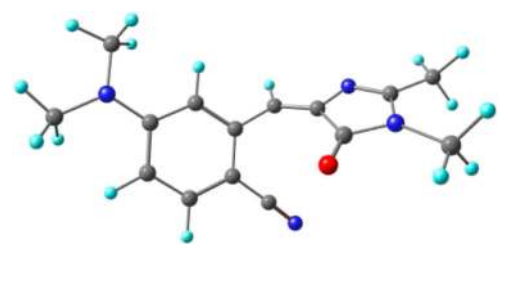
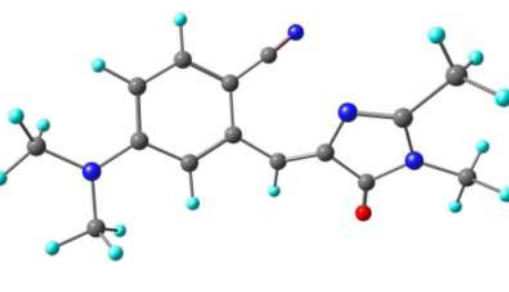
Materials

The structures of the uGFPc studied here are shown in **Figure 1A**. The details of the molecular design, synthesis process, and electronic spectroscopic studies of these molecules are reported elsewhere (26). The design concept relies on the fact that the τ -torsion [i.e., the $Z^* \rightarrow {}^1p^*$ reaction in the $Z \rightarrow E$ photoisomerization coordinate of the one-bond-flip mechanism (31)] is the principal non-radiative decay pathway for **1**. Destabilizing the reactive intermediate can raise the reaction barrier and slow down the process (32). By adding an electron-withdrawing group to the places in the resonance structures that bear a positive charge, it was claimed that the ${}^1p^*$ state may be destabilized to further enhance the τ -torsion barrier in favor of fluorescence emission. In this context, the strong electron-withdrawing and linear-shaped CN groups were chosen, and for the synthetic feasibility, the CN substituent was designed to locate on the aniline moiety rather than on the exocyclic carbon. We have used the spectroscopy-grade anhydrous DMF solvent to prepare its dilute solution samples of concentration ~ 0.05 mM. UV-visible absorption spectra of the solutions were measured using a commercial UV-Vis spectrometer.

Femtosecond Z-Scan Studies

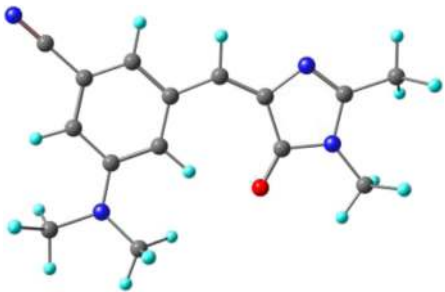
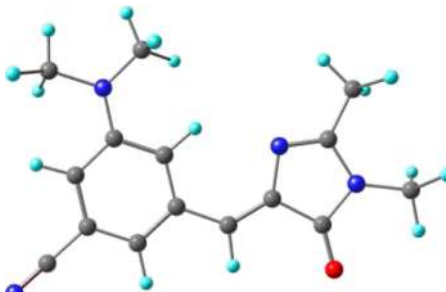
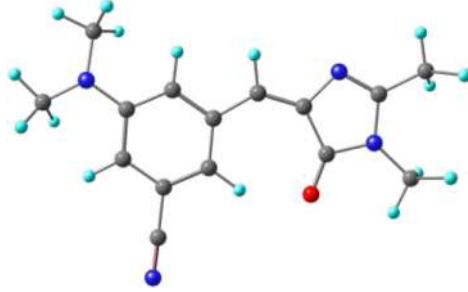
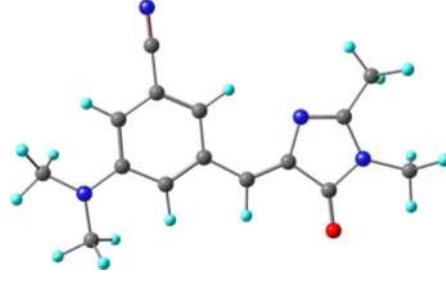
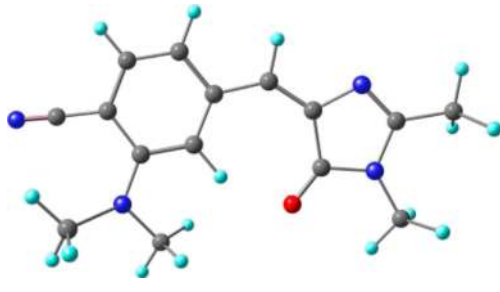
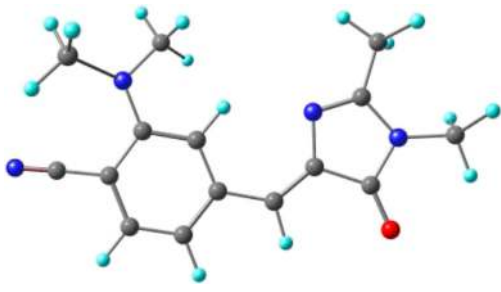
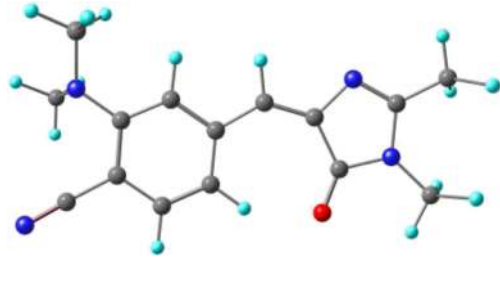
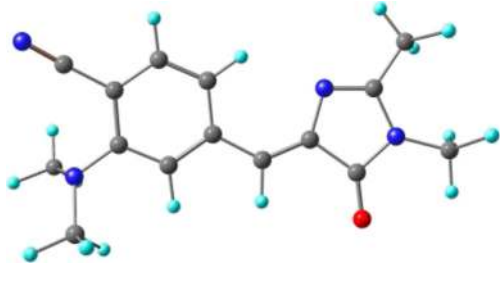
The conventional Z-scan setup (33–35) was used to execute the fs Z-scan studies. A Ti:sapphire laser amplifier (LIBRA, Coherent,

TABLE 1 | Optimized geometry and relative energies (REs, kcal) of all the possible isomers at B3LYP/6-31G (d, p).

Molecule	E-isomer (RE)	Z-isomer (RE)
1	 <p>E1 (2.25)</p>	 <p>Z1 (0.00)</p>
	 <p>E2 (3.35)</p>	 <p>Z2 (0.47)</p>
2	 <p>E1 (2.00)</p>	 <p>Z1 (0.00)</p>
	 <p>E2 (7.92)</p>	 <p>Z2 (5.54)</p>

(Continued on following page)

TABLE 1 | (Continued) Optimized geometry and relative energies (REs, kcal) of all the possible isomers at B3LYP/6-31G (d, p).

Molecule	E-isomer (RE)	Z-isomer (RE)
3	 E1 (2.18)	 Z1 (0.00)
	 E2 (3.57)	 Z2 (0.27)
4	 E1 (2.47)	 Z1 (0.00)
	 E2 (3.23)	 Z2 (0.27)

In **Table 1**, E and Z are isomers and the value inside bracket is the relative energy of the corresponding isomer in "kcal" unit.

Inc.) seeded by an oscillator was used as a light source. A part of the laser output from the amplifier having a central wavelength of 800 nm, ~70 fs pulse duration, and 1 kHz repetition rate was used for

the measurements. The laser beam was focused over the sample by using a plano-convex lens of focal length ~ 15 cm. At the focus, the estimated beam waist was ~32 μM , and the estimated peak

TABLE 2 | Absorption energies (λ in nm), oscillator strength (f), % contribution (% Ci), and major transitions (MTs) obtained at the TD-CAMB3LYP/6-311+G (d, p) level.

Molecules	λ_{exp} (nm)	States	λ (nm)	f	%Ci	MT
1-Z1	376	S1	375	0.284	94	H \rightarrow L
	354	S2	337	0.505	97	H-1 \rightarrow L
	295	S3	297	0.001	93	H-3 \rightarrow L
2-Z1	377	S1	374	0.193	94	H \rightarrow L
	351	S2	350	0.535	96	H-1 \rightarrow L
	303	S3	308	0.0004	93	H-3 \rightarrow L
3-Z1	374	S1	377	0.261	91	H \rightarrow L
	352	S2	339	0.484	94	H-1 \rightarrow L
	309	S3	302	0.001	90	H-3 \rightarrow L
4-Z1	370	S1	375	0.457	93	H \rightarrow L
	355	S2	351	0.448	95	H-1 \rightarrow L
	305	S3	309	0.001	88	H-3 \rightarrow L

intensity was $\sim 300 \text{ GW/cm}^2$. The corresponding Rayleigh range (Z_0) was calculated and found to be $\sim 4 \text{ mm}$. The solution samples were placed in a quartz cuvette with a path length of $\sim 1 \text{ mm}$, and the cuvette was placed on a motorized stage (for scanning the sample) using a sample holder. The stage was translated along the Z direction, and the sample was scanned to the positive and negative sides of the $Z = 0$ position. The transmitted signal through the samples was collected by a silicon photodiode (PD-Thorlabs) which was connected to the lock-in amplifier. The motorized stage was functioned using a motion controller (Newport-ESP 300), and the lock-in amplifier was integrated with this motion controller *via* the LabVIEW interface. One can measure the multi-photon absorption of the samples by scanning the samples in the focal plane of the lens without placing an aperture or by placing an open aperture at the photodiode (OA). The aperture at the far-field position before the photodiode was closed to make the transmitted signal sensitive to the central part of the beam profile for the closed-aperture (CA) Z-scan study. Important parameters such as the intensity-dependent non-linear refraction (n_2) and the real part of third-order non-linear susceptibility [$\chi^{(3)}$] are determined by the CA Z-scan studies. The input peak intensity was selected such that the impact of pure solvent was negligible and it was confirmed from the Z-scan measurements of pure solvent alone, which exhibited negligible NLO transmittance. During the measurements of all the samples, a linear transmittance of 90–96% at 800 nm was noted. An estimated error of $\pm 5\%$ due to the backlash error of the stage, estimation of intensity as a function of distance Z, and input laser energy fluctuations is expected in the NLO coefficients obtained from these measurements.

Density Functional Theory Calculations

All the reported molecules were optimized at the B3LYP/6-31G (d, p) level of theory. The frequencies of the optimized geometries were evaluated at the same level, and it was found that the structures were minima on the potential energy surface. Each molecule existed in four stable conformers named as E1, E2, Z1, and Z2 (two in the E isomer and two in the Z isomer) on the potential energy surface. Out of the four conformers, the Z1 isomer was the most stable one for all the molecules, and the

detailed molecular structures along with its relative energies are summarized in **Table 1**. Further calculations such as electronic excitations and NLO properties are reported for the most stable structure Z1. All the calculations were carried out using G 16 W software (36).

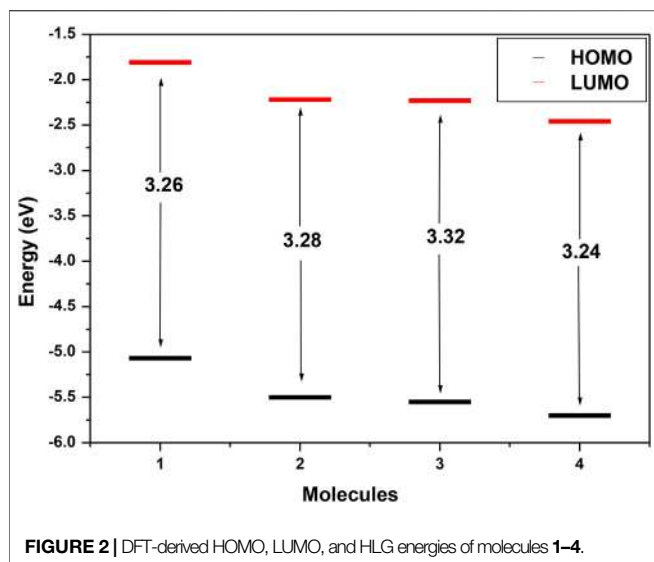
RESULTS AND DISCUSSION

Figure 1B presents the absorption spectra of the molecules **1**, **2**, **3**, and **4**, in solution of DMF, depicting peaks near 354 nm, 367 nm, 355 nm, and 370 nm, respectively. The absorption profiles for all the samples were found to be similar, and each consisted of a BDI-based locally excited (LE) $\pi - \pi^*$ transition band near 360 nm and a wide shoulder, with absorption up to 480 nm, ascribable to the aniline-to-imidazolinone charge-transfer (CT) transition (30). Therefore, it is expected to demonstrate strong NLO properties by these uGFPc due to the presence of π -electron distribution. Using the open-aperture Z-scan technique, the non-linear (multi-photon) absorption properties were evaluated, and the third-order non-linear refractive index response and second hyperpolarizability of these molecules were also appraised by employing the closed-aperture Z-scan technique.

To gain an understanding of the observed absorption energies, TDDFT calculations were performed at TD-CAMB3LYP/6-311+G (d, p) with the inclusion of solvent DMF. The TDDFT-derived transitions along with contributions (in %Ci) are summarized in **Table 2**. It is clear from **Table 2** that all the molecules' parameters obtained are in good agreement with the experimental observations. The major transitions are from HOMO to LUMO in its first excitation (S1), whereas the second (S2) and third (S3) excitations are from HOMO-1 to LUMO and from HOMO-3 to LUMO, respectively. The electron density is mainly localized on the benzene part in the HOMO and on the acceptor imidazolinone part in the LUMO. The stabilization in HOMO and LUMO levels was observed from the unsubstituted molecule **1** to substituted molecules **2**, **3**, and **4** (**Figure 2**). Molecule **4** (ortho-substituted) has deeper HOMO and LUMO levels with a smaller HOMO–LUMO gap (HLG) of 3.24 eV among the four molecules.

Open-Aperture Z-Scan

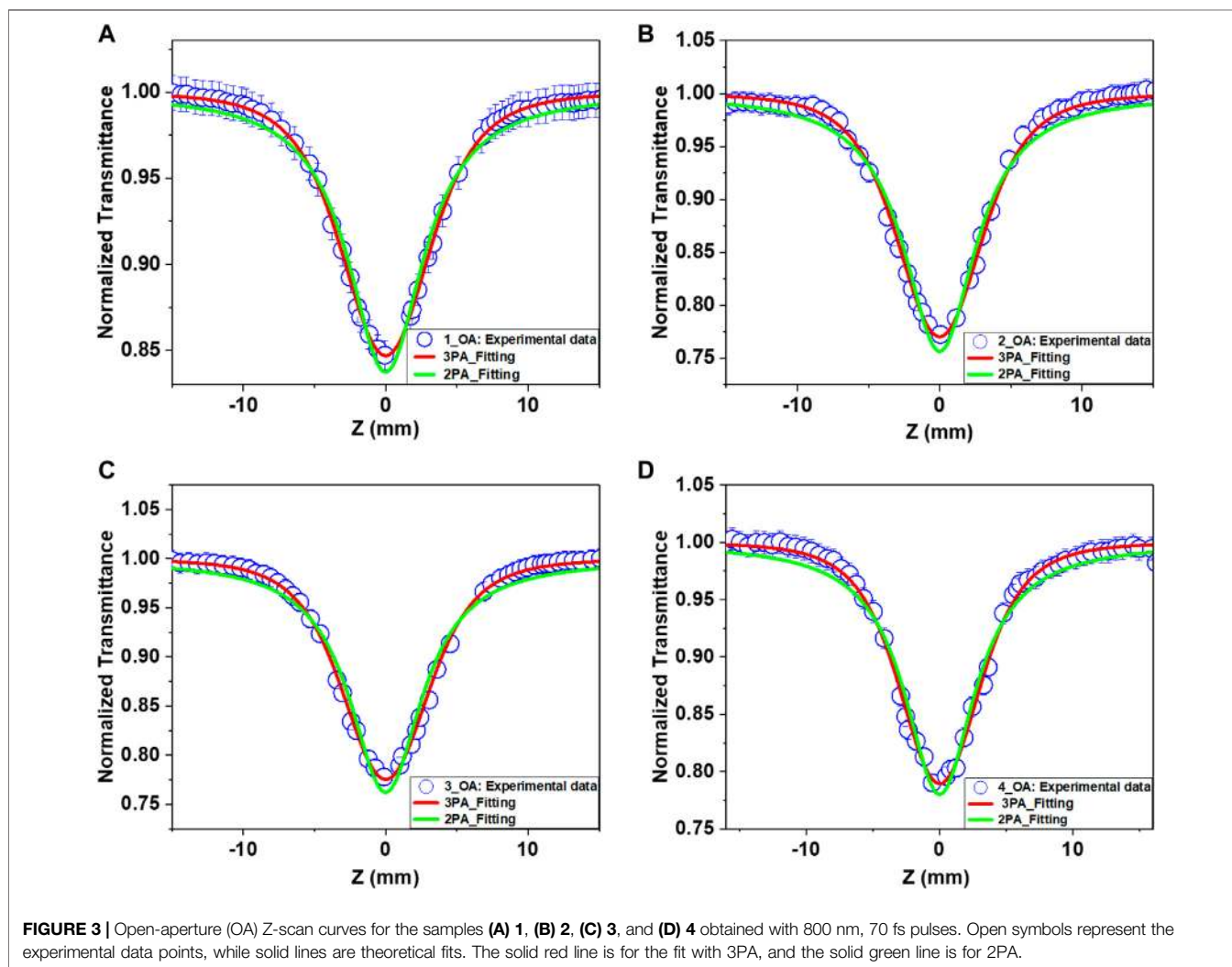
Symmetric transmission plots, shown in **Figure 3**, are the OA Z-scan curves measured at the wavelength of 800 nm. Since the intensity of the input beam increased toward $Z = 0$ position, the transmission through the sample declined and finally saturated with higher input intensities. The data found for all the samples at different input intensities stipulate a reverse saturable absorption (RSA) behavior. Generally, in any molecule, if the excited-state absorption is larger than the ground-state absorption, it allows them to exhibit prominent RSA response. A photon is absorbed from a singlet level (S_1) or a triplet level (T_1) to a higher level in this condition. A reverse saturation phenomenon occurs when the cross section of either the $S_1 - S_2$ or $T_1 - T_2$ transition is bigger than that of the ground state (37). RSA can result in strong absorption by the non-linear absorber at high input intensities/energy densities of the



incident laser (38) and low absorption at low input intensities/energy densities of the incident laser. However, transparency at low input energy but a very strong absorption at high input

energy can be achieved with multi-photon absorption (MPA) in which “*n*” photons are absorbed simultaneously. In the present case, the incident, laser intensities were optimized to avoid supercontinuum generation.

It is not possible to trigger a direct electronic transition from the ground state to the excited state *via* one-photon absorption under our experimental conditions because the energy of the excitation light (1.55 eV) is shorter than the energy gap (E_g) of these uGFPc (Figure 2). More specifically, we have seen a negligible one-photon absorption at the excitation wavelength of 800 nm for all the molecules. Thus, the only possibility for electrons to reach the excited state is *via* MPA. Due to the large peak intensities at the focus with fs laser pulses, either two-photon absorption (2PA) or three-photon absorption (3PA) can be expected as the possible non-linear absorption mechanism. The condition for the 3PA is described as $2 \text{ h}\nu < E_g < 3 \text{ h}\nu$ (39). The photon energy $3 \text{ h}\nu$ corresponding to 800 nm (4.65 eV) is sufficient for population transition by the ground-state absorption. Therefore, it is an indication that the optical non-linearity observed at non-resonant excitation could be attributed to the generation of free or bound carriers *via* most likely the 3PA process.



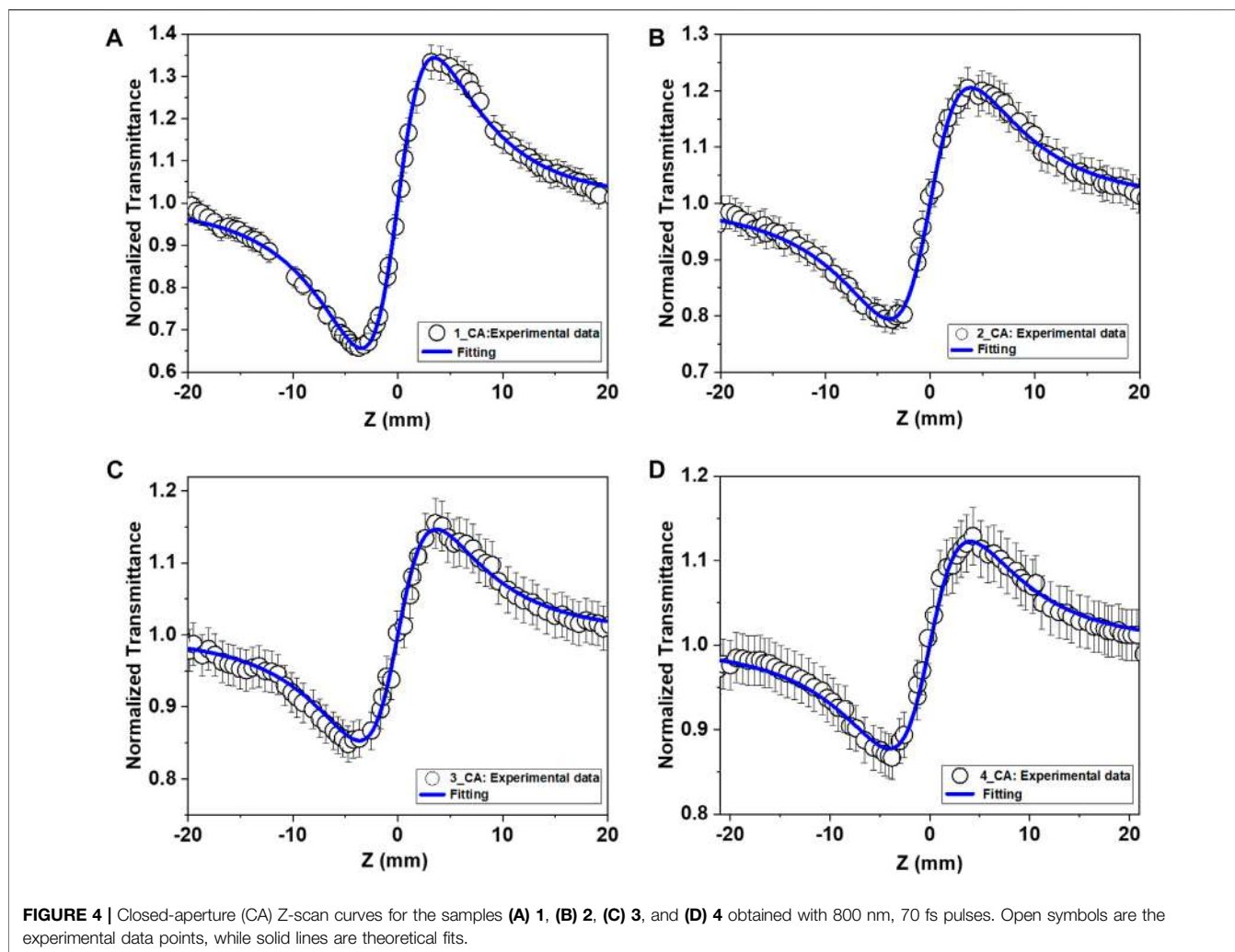


FIGURE 4 | Closed-aperture (CA) Z-scan curves for the samples (A) 1, (B) 2, (C) 3, and (D) 4 obtained with 800 nm, 70 fs pulses. Open symbols are the experimental data points, while solid lines are theoretical fits.

TABLE 3 | NLO parameters of the investigated molecules obtained from OA, CA Z-scan, and DFT studies.

Sample	α_3 (cm^3/GW^2) $\times 10^{-5}$	n_2 (cm^3/W^2) $\times 10^{-16}$	$\chi_R^{(3)}$ (esu) $\times 10^{-14}$	γ (esu) $\times 10^{-33}$	DFT-derived γ (esu) $\times 10^{-33}$	Optical-limiting onset (mJ/cm^2)
1	3.31	7.18	3.73	6.07	1.66	3.85
2	5.75	4.30	2.23	3.63	0.76	3.90
3	5.57	3.07	1.59	2.59	1.43	3.92
4	5.08	2.57	1.33	2.17	2.97	3.93

TABLE 4 | Comparison of the values of obtained second hyperpolarizability with those in the published works.

Compound	Laser pulse width, wavelength (used method)	γ (esu)	References
uGFPc	~70 fs, 800 nm (Z-scan)	$(2.17 - 6.07) \times 10^{-33}$	Current work
Quinoxalines	~70 fs, 800 nm (degenerate four-wave mixing (DFWM))	$\sim 10^{-31}$	(50)
Orthogonal pyrrolotetrafulvalene derivatives (S1, S2, S3)	30 ps, 532 nm (Z-scan)	$\sim 10^{-31}$	(53)
NLOphoric mono-azo dyes	(DFT, solvatochromism)	$\sim 10^{-33}$, $\sim 10^{-34}$, $\sim 10^{-35}$	(54)
Croconate dyes	100 fs, 800 nm (DFWM)	-2.4 to -5.3×10^{-32}	(55)
Squaraine dyes	210 fs and 3 ps; 696 and 710 nm (DFWM)	$\sim 8 \times 10^{-32}$	(56)
Methyl orange dyes (azo dyes)	(Monte Carlo/DFT)	$\sim 10^{-34}$	(57)
Azo dye	5 ns, 532 nm (Z-scan)	$\sim 10^{-35}$	(58)
HMB	(Z-scan)	0.5×10^{-35}	(59)

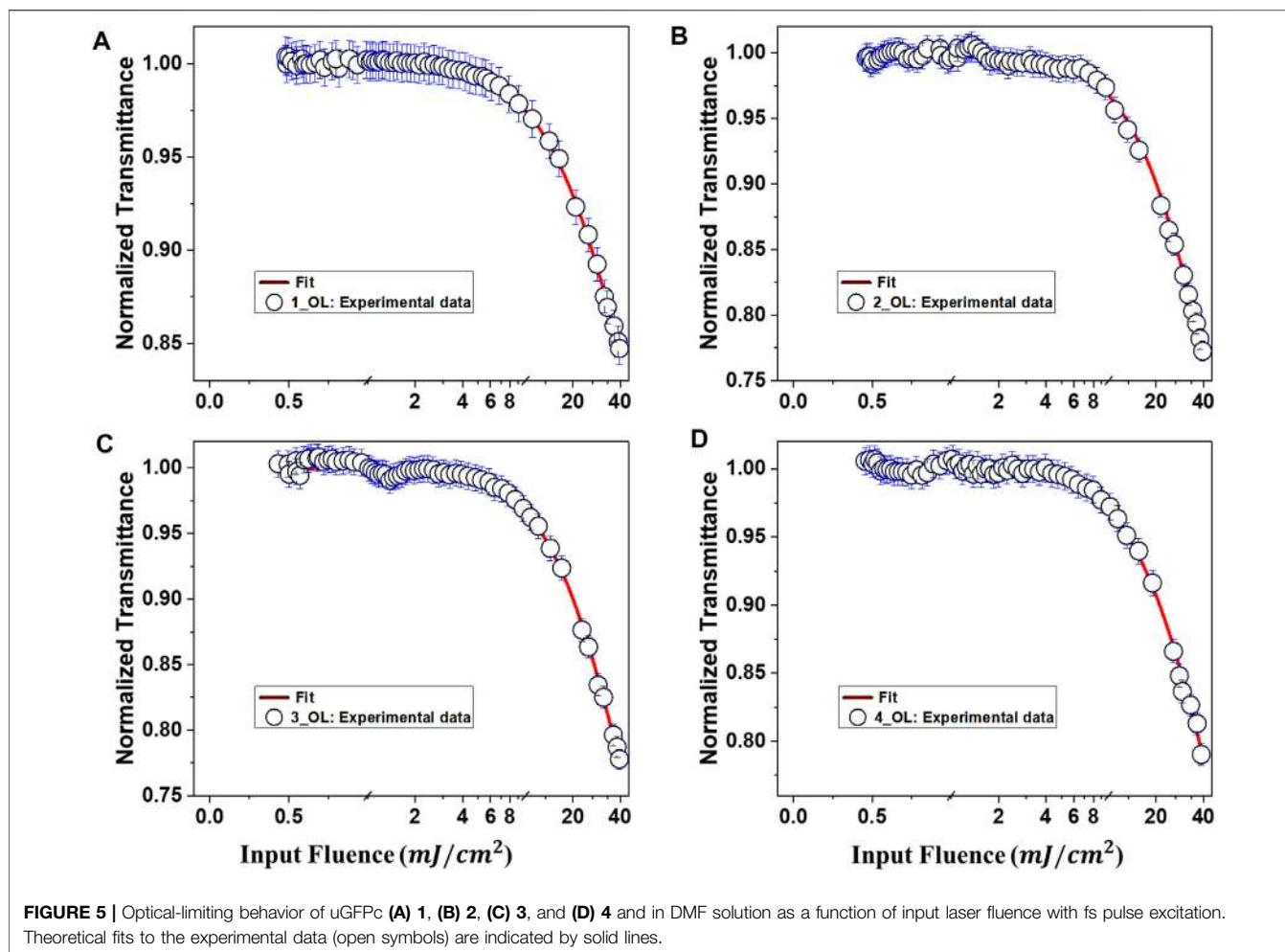


TABLE 5 | Optical-limiting onset threshold of different molecules studied.

Name of the compound	Pulse width, wavelength	Optical-limiting onset (J/cm ²)	References
Oleylamine-capped gold nanoparticles	7 ns, 1064 nm and 7 ns, 532 nm	7.5 and 0.6	(61)
CNTs	7 ns, 1064 nm and 7 ns, 532 nm	10.0 and 1.0	(61)
PC3	2 ps, 800 nm	11.2×10^{-2}	(62)
Ag PNC films	150 fs, 800 nm	3.8×10^{-2}	(63)
DMMC	150 fs, 800 nm	5.6×10^{-3}	(60)
G1, G3	70 fs, 800 nm	$\sim 5.8 \times 10^{-3}$	(35)
uGFPc	70 fs, 800 nm	$\sim 4 \times 10^{-3}$	Current work

Assuming the Gaussian beam profile, the general equation for normalized energy transmittance given by Sutherland et al. (33, 34, 40) using the open-aperture Z-scan theory for multi-photon absorption is described as

$$T_{OA(nPA)} = \frac{1}{\left[1 + (n-1)\alpha_n L_{eff} \left(\frac{I_0}{1 + \left(\frac{z}{z_0}\right)^2} \right)^{n-1} \right]} \quad (1)$$

where α_n is the non-linear MPA coefficient of the sample such as $n = 2$ for two-photon absorption (2PA), $n = 3$ for 3PA, and so on. L_{eff} is the effective path length of the sample, $z_0 = \frac{\pi\omega_0^2}{\lambda}$ is the Rayleigh range, z is the sample position with respect to the focusing lens, ω_0 is the beam width at the focal point, and I_0 is the input peak irradiance at the focus.

We employed the following analytical equations for fitting the 2PA and 3PA to OA Z-scan data by choosing $n = 2$ and $n = 3$:

$$T_{oA(2PA)} = \frac{1}{1 + \alpha_2 L_{eff} \left(\frac{I_0}{1 + (z/z_0)} \right)}, \quad (2)$$

$$T_{OA(3PA)} = \frac{1}{\left[1 + 2\alpha_3 L_{eff}' \left(\frac{I_0}{1 + \left(\frac{z}{z_0} \right)^2} \right) \right]^{2.75}} \quad (3)$$

Here, α_2 is the 2PA coefficient and α_3 is the 3PA coefficient. $L_{eff} = \frac{1 - e^{-\alpha_0 L}}{\alpha_0}$ and $L_{eff}' = \frac{1 - e^{-2\alpha_0 L}}{2\alpha_0}$ are the effective path length of the sample for 2PA and 3PA, respectively, where α_0 is the linear absorption coefficient. The calculated value of the effective path length (~ 0.99 mm) is found to be much smaller than the Rayleigh range, which satisfies the thin-film approximation $L_{eff} \ll z_0$ (41). In **Figure 3**, we found that the obtained experimental data were satisfactorily fitted using the transmission equation for 3PA [equation (3)]. In other words, the superior mechanism for observed RSA is 3PA. Two-photon absorption followed by excited-state absorption is another possibility (42). Therefore, this non-linearity is referred to as an “effective 3PA” process. The values for the 3PA coefficient for samples **1**, **2**, **3**, and **4** were $3.31 \times 10^{-05} \text{ cm}^3/\text{GW}^2$, $5.75 \times 10^{-05} \text{ cm}^3/\text{GW}^2$, $5.57 \times 10^{-05} \text{ cm}^3/\text{GW}^2$, and $5.08 \times 10^{-05} \text{ cm}^3/\text{GW}^2$, respectively. The strong 3PA coefficients of these molecules indicate that these molecules can be used for three-photon imaging (3PI), which is found to be advantageous to obtain the clear images of tissue (43–45). The longer wavelength of the light allows it to penetrate deeper into tissue. Light scatters less, allowing for clear pictures of structures deep within scattering tissue. Fluorophores deeper in tissue can be activated, and structures can be viewed in 3D.

Closed-Aperture Z-Scan

Next, we employed the closed-aperture (CA) Z-scan measurements on the uGFPC. To extract the non-linear parameters, the CA Z-scan data were fitted by the following acknowledged formula (46):

$$T_{CA}(x) = 1 + \frac{4x\Delta\Phi}{(1+x^2)(9+x^2)} + \frac{4(3x^2-5)\Delta\Phi^2}{(1+x^2)(9+x^2)(25+x^2)} + \frac{32(3x^2-11)x\Delta\Phi^3}{(1+x^2)(9+x^2)(25+x^2)(49+x^2)} \quad (4)$$

where $T_{CA}(x)$ is the normalized transmittance of the CA study, $x = -z/z_0$, z is the longitudinal displacement of the sample from the focal point ($z = 0$), and z_0 is the Rayleigh diffraction length. From the fitted curve, we primarily obtained the on-axis non-linear phase shift at the focus $\Delta\Phi$. Again, due to the presence of intense laser beam in the third-order NLO medium, the non-linear refractive index (n_2) comes into the picture to modify the refractive index of the medium (47). The relationship between the non-linear phase shift and the non-linear refractive index is expressed as

$$\Delta\Phi = kn_2 I_0 L_{eff} \quad (5)$$

where $k = 2\pi/\lambda$ is the wave vector, I_0 is the laser radiance at the focus, and L_{eff} is the effective length of the sample. From the

difference between the normalized peak and the valley transmittance (ΔT_{p-v}) in the CA Z-scan data (33, 48), the non-linear refractive index was estimated:

$$\Delta T_{p-v} = 0.406(1-S)^{0.25} \Delta\Phi \quad (6)$$

where S is the linear transmittance of the aperture: $S = 1 - \exp(-2r_a^2/w_a^2)$, w_a is the radius of the laser spot before the aperture, and r_a is the radius of the aperture. The CA curves (**Figure 4**) of all the samples exhibited a valley-peak structure. These curves were normalized by dividing CA data by OA data to eliminate the contribution of MPA. The observed pre-focal transmission minimum (valley) followed by a transmission maximum (peak) stands for the signature of positive non-linearity with the non-linear refractive index, $n_2 > 0$. The magnitude of the non-linear refractive index was obtained using **Eq. 5**. The estimated values of n_2 were $7.18 \times 10^{-16} \text{ cm}^2/\text{W}$, $4.3 \times 10^{-16} \text{ cm}^2/\text{W}$, $3.07 \times 10^{-16} \text{ cm}^2/\text{W}$, and $2.57 \times 10^{-16} \text{ cm}^2/\text{W}$, respectively, for molecules **1**, **2**, **3**, and **4**.

The third-order non-linear susceptibility is a complex quantity (14): $\chi^{(3)} = \chi_R^{(3)} + i\chi_I^{(3)}$, where the real part ($\chi_R^{(3)}$) is related to n_2 and the imaginary part ($\chi_I^{(3)}$) is related to 2PA coefficient (33). We have calculated the real part of the third-order non-linear susceptibility using the following relation (49):

$$\chi_R^{(3)} (\text{esu}) = \frac{10^{-4} \epsilon_0 C^2 n_0^2 n_2 (\text{cm}^2 \text{W}^{-1})}{\pi} \quad (7)$$

Here, c is the speed of the light and n_0 is the linear refractive index of the sample. Because the exact value of n_0 for these samples is not known, we have taken the value $n_0 = 1.43$ of DMF, the solvent of the samples. As all the molecules have demonstrated 3PA and only $\chi_R^{(3)}$ has dominant contribution to the third-order non-linear susceptibility of the molecules, using the values of NLO susceptibility, we have evaluated the values of second hyperpolarizability $\langle \gamma \rangle$ (50). The relation (35, 51) used to determine $\langle \gamma \rangle$ is expressed as

$$\langle \gamma \rangle = \frac{\chi^{(3)}}{L^4 N} \quad (8)$$

in which $L = \frac{n_0^2 + 2}{3}$ is the local field factor and N is the number density of the molecules in solution samples. The calculated values of n_2 , $\chi_R^{(3)}$, and $\langle \gamma \rangle$ for all the molecules are listed in **Table 3**.

The average second hyperpolarizability values γ are obtained for all the molecules using various DFT functionals (TD-CAMB3LYP) based on B3LYP/6-31G (d, p) optimized geometries. The γ values were calculated using two-state models (52), and the γ was evaluated for each molecule using the transition dipole moment and the excitation energy obtained in DMF by TD-CAMB3LYP. The calculated results are in good agreement with the experimental findings (**Table 3**). All the molecules have demonstrated magnitude of γ values $\sim 10^{-33} \text{ esu}$. The non-resonant NLO γ values for these uGFPC were found to be higher than or comparable to those of the previously reported materials. We have shown the comparison in **Table 4**.

Optical Limiting

An excellent optical limiter behaves as a transparent medium at low input intensities and an opaque medium for high input fluence. The transmittance of the medium decreases with the increasing input laser intensity or fluence in the optical-limiting medium. The intensity-dependent transmission is utilized in this way to keep the transmitted light intensity below a certain level. Optical limiters are used to protect the human eyes, light-sensitive optical elements, and optical sensors from damages induced by intense laser pulse fluence (60). The normalized transmittance of the molecules in DMF solution as a function of input laser fluence is illustrated in **Figure 5**. The input laser fluence was calculated from the OA Z-scan data since for a Gaussian beam, each Z location of the sample corresponds to an input beam fluence following the relation (40, 60):

$$E(z) = \frac{4\sqrt{\ln 2}E_{in}}{\pi^2\omega^2(z)}, \quad (9)$$

where E_{in} is the input laser pulse energy and $\omega(z)$ is the beam radius with respect to the z-position.

From **Figure 5**, it is noticed that the deviation from linear transmittance for **1**, **2**, **3**, and **4** is happening at an input fluence of $3.9 \times 10^{-3} \text{ J/cm}^2$, $4.2 \times 10^{-3} \text{ J/cm}^2$, $4 \times 10^{-3} \text{ J/cm}^2$, and $4.1 \times 10^{-3} \text{ J/cm}^2$, respectively. This deviation of linear transmittance suggested the occurrence of optical limiting in uGFPc. The values of input fluence where the deviation from linear transmittance occurred are enlisted in **Table 5**. The optical-limiting (OL) onset values suggested that these organic molecules are potential candidates for the optical-limiting applications as these molecules have lower OL onset values. For comparison, OL values for different molecules are tabulated in **Table 5**.

CONCLUSIONS

The non-resonant NLO properties of the four uGFPc **1–4** have been investigated by the femtosecond Z-scan technique. We performed the open-aperture and closed-aperture Z-scan studies with 800 nm, 100 fs pulses to characterize the ultrafast third-order optical non-linearity in detail. From the

HOMO–LUMO gap (DFT calculations) and OA Z-scan curves of the molecules, we conclude that these molecules exhibit three-photon absorption and reverse saturable absorption behavior. These features indicated the application of these molecules in three-photon microscopy in the future. In addition, the optical-limiting properties, third-order non-linear absorption coefficients, and non-linear refractive indices were estimated. We evaluated third-order non-linear susceptibilities and second hyperpolarizability and verified these values with theoretical calculations. We conclude that, with a non-centrosymmetric structure, visible-light absorption, and larger γ values, these GFPs might find particular utility in NLO applications.

DATA AVAILABILITY STATEMENT

The original contributions presented in the study are included in the article/Supplementary Material, and further inquiries can be directed to the corresponding authors.

AUTHOR CONTRIBUTIONS

MA and CB measured and analyzed steady-state photophysics and NLO measurements. DB supported with femtosecond laser setup and data collection. PC performed DFT calculations. J-SY provided the molecules for study. VS provided the laser support and was involved in data analysis. SR supervised the entire project in terms of data curation and analysis and project funding. All authors contributed equally in writing and reviewing the manuscript.

FUNDING

MA and SR acknowledge the financial support of BRICS/PilotCall2/IEEE-OSC/2018 (G) and CRG/2019/003197, respectively, and J-SY thanks the financial support of MOST of Taiwan (MOST 110-2113-M-002-011-MY3).

REFERENCES

- De Meulenaere E, de Coene Y, Russier-Antoine I, Vanpraet L, Van den Haute C, Thevissen K, et al. Fluorescence-free First Hyperpolarizability Values of Fluorescent Proteins and Channel Rhodopsins. *J Photochem Photobiol A: Chem* (2020) 400:112658. doi:10.1016/j.jphotochem.2020.112658
- Dedecker P, De Schryver FC, Hofkens J. Fluorescent Proteins: Shine on, You Crazy diamond. *J Am Chem Soc* (2013) 135(7):2387–402. doi:10.1021/ja309768d
- Shaner NC, Steinbach PA, Tsien RY. A Guide to Choosing Fluorescent Proteins. *Nat Methods* (2005) 2(12):905–9. doi:10.1038/nmeth819
- Shimomura O, Johnson FH, Saiga Y. Extraction, Purification and Properties of Aequorin, a Bioluminescent Protein from the Luminous Hydromedusan, Aequorea. *J Cell Comp Physiol* (1962) 59(3):223–39. doi:10.1002/jcp.1030590302
- Potter SM, Wang C-M, Garrity PA, Fraser SE. Intravital Imaging of green Fluorescent Protein Using Two-Photon Laser-Scanning Microscopy. *Gene* (1996) 173(1):25–31. doi:10.1016/0378-1119(95)00681-8
- Volkmer A, Subramaniam V, Birch DJ, Jovin TM. One-and Two-Photon Excited Fluorescence Lifetimes and Anisotropy Decays of green Fluorescent Proteins. *Biophysical J* (2000) 78(3):1589–98. doi:10.1016/s0006-3495(00)76711-7
- Prasad PN, Williams DJ. *Introduction to Nonlinear Optical Effects in Molecules and Polymers*. New York: Wiley (1991).
- Williams DJ. Organic Polymeric and Non-polymeric Materials with Large Optical Nonlinearities. *Angew Chem Int Edition English* (1984) 23(9):690–703. doi:10.1002/anie.198406901
- Zyss J, Ledoux I. Nonlinear Optics in Multipolar media: Theory and Experiments. *Chem Rev* (1994) 94(1):77–105. doi:10.1021/cr00025a003
- Karna SP, Yeates AT. *Nonlinear Optical Materials: Theory and Modeling*. Washington, DC: ACS Publications (1996).

11. Zyss J. *Molecular Nonlinear Optics: Materials, Physics, and Devices*. Massachusetts(United States): Academic Press (2013).
12. Sutherland R. *Handbook of Nonlinear Optics*. New York: Marcel Dekker (1996).
13. Verbiest T, Houbrechts S, Kauranen M, Clays K, Persoons A. Second-order Nonlinear Optical Materials: Recent Advances in Chromophore Design. *J Mater Chem* (1997) 7(11):2175–89. doi:10.1039/a703434b
14. Boyd RW. *Nonlinear Optics*. Massachusetts(United States): Academic Press (2020).
15. Bredas J-L, Adant C, Tackx P, Persoons A, Pierce B. Third-order Nonlinear Optical Response in Organic Materials: Theoretical and Experimental Aspects. *Chem Rev* (1994) 94(1):243–78. doi:10.1021/cr00025a008
16. Nakano M, Kishi R, Ohta S, Takebe A, Takahashi H, Furukawa S, et al. Origin of the Enhancement of the Second Hyperpolarizability of Singlet Diradical Systems with Intermediate Diradical Character. *J Chem Phys* (2006) 125(7):074113. doi:10.1063/1.2213974
17. Nakano M, Kubo T, Kamada K, Ohta K, Kishi R, Ohta S, et al. Second Hyperpolarizabilities of Polycyclic Aromatic Hydrocarbons Involving Phenalenyl Radical Units. *Chem Phys Lett* (2006) 418(1-3):142–7. doi:10.1016/j.cplett.2005.10.109
18. Ohta S, Nakano M, Kubo T, Kamada K, Ohta K, Kishi R, et al. Second Hyperpolarizability of Phenalenyl Radical System Involving Acetylene π -conjugated Bridge. *Chem Phys Lett* (2006) 420(4-6):432–7. doi:10.1016/j.cplett.2006.01.022
19. Srinivas K, Prabhakar C, Devi CL, Yesudas K, Bhanuprakash K, Rao VJ. Enhanced Diradical Nature in Oxyallyl Derivatives Leads to Near Infra Red Absorption: A Comparative Study of the Squaraine and Croconate Dyes Using Computational Techniques. *The J Phys Chem A* (2007) 111(17):3378–86. doi:10.1021/jp067410f
20. De Meulenaere E, Asselberghs I, De Wergifosse M, Botek E, Spaepen S, Champagne B, et al. Second-order Nonlinear Optical Properties of Fluorescent Proteins for Second-Harmonic Imaging. *J Mater Chem* (2009) 19(40):7514–9. doi:10.1039/b907789h
21. De Meulenaere E, Nguyen Bich N, de Wergifosse M, Van Hecke K, Van Meervelt L, Vanderleyden J, et al. Improving the Second-Order Nonlinear Optical Response of Fluorescent Proteins: the Symmetry Argument. *J Am Chem Soc* (2013) 135(10):4061–9. doi:10.1021/ja400098b
22. Reeve JE, Collins HA, Mey KD, Kohl MM, Thorley KJ, Paulsen O, et al. Amphiphilic Porphyrins for Second Harmonic Generation Imaging. *J Am Chem Soc* (2009) 131(8):2758–9. doi:10.1021/ja8061369
23. De Wergifosse M, Botek E, De Meulenaere E, Clays K, Champagne B. ONIOM Investigation of the Second-Order Nonlinear Optical Responses of Fluorescent Proteins. *The J Phys Chem B* (2018) 122(19):4993–5005. doi:10.1021/acs.jpbc.8b01430
24. Asselberghs I, Flors C, Ferrighi L, Botek E, Champagne B, Mizuno H, et al. Second-harmonic Generation in GFP-like Proteins. *J Am Chem Soc* (2008) 130(46):15713–9. doi:10.1021/ja805171q
25. Tsai M-S, Lee C-H, Hsiao J-C, Sun S-S, Yang J-S. Solvatochromic Fluorescence of a GFP Chromophore-Containing Organogelator in Solutions and Organogels. *J Org Chem* (2021) 87:1723–31. doi:10.1021/acs.joc.1c01911
26. Tsai M-S, Ou C-L, Tsai C-J, Huang Y-C, Cheng Y-C, Sun S-S, et al. Fluorescence Enhancement of Unconstrained GFP Chromophore Analogues Based on the Push–Pull Substituent Effect. *J Org Chem* (2017) 82(15):8031–9. doi:10.1021/acs.joc.7b01260
27. Wu L, Burgess K. Syntheses of Highly Fluorescent GFP-Chromophore Analogues. *J Am Chem Soc* (2008) 130(12):4089–96. doi:10.1021/ja710388h
28. Chuang W-T, Hsieh C-C, Lai C-H, Lai C-H, Shih C-W, Chen K-Y, et al. Excited-state Intramolecular Proton Transfer Molecules Bearing O-Hydroxy Analogues of green Fluorescent Protein Chromophore. *J Org Chem* (2011) 76(20):8189–202. doi:10.1021/jo2012384
29. Hsu Y-H, Chen Y-A, Tseng H-W, Zhang Z, Shen J-Y, Chuang W-T, et al. Locked Ortho-And Para-Core Chromophores of green Fluorescent Protein; Dramatic Emission Enhancement via Structural Constraint. *J Am Chem Soc* (2014) 136(33):11805–12. doi:10.1021/ja5062856
30. Huang G-J, Ho J-H, Prabhakar C, Liu Y-H, Peng S-M, Yang J-S. Site-selective Hydrogen-Bonding-Induced Fluorescence Quenching of Highly Solvatofluorochromic GFP-like Chromophores. *Org Lett* (2012) 14(19):5034–7. doi:10.1021/ol302237k
31. Dugave C. *cis-trans Isomerization in Biochemistry*. New Jersey(United States): John Wiley & Sons (2006).
32. Hammond GS. A Correlation of Reaction Rates. *J Am Chem Soc* (1955) 77(2):334–8. doi:10.1021/ja01607a027
33. Sheik-Bahae M, Said AA, Wei T-H, Hagan DJ, Van Stryland EW. Sensitive Measurement of Optical Nonlinearities Using a Single Beam. *IEEE J Quan Electron* (1990) 26(4):760–9. doi:10.1109/3.53394
34. Kumar RSS, Rao SV, Giribabu L, Rao DN. Femtosecond and Nanosecond Nonlinear Optical Properties of Alkyl Phthalocyanines Studied Using Z-Scan Technique. *Chem Phys Lett* (2007) 447(4-6):274–8. doi:10.1016/j.cplett.2007.09.028
35. Biswas C, Katturi NK, Duvva N, Giribabu L, Soma VR, Raavi SSK. Multistep Electron Injection Dynamics and Optical Nonlinearity Investigations of π -Extended Thioalkyl-Substituted Tetrathiafulvalene Sensitizers. *The J Phys Chem C* (2020) 124(44):24039–51. doi:10.1021/acs.jpcc.0c06010
36. Gaussian09 RA 1Frisch MJ, Trucks GW, Schlegel HB, Scuseria GE, Robb MA, et al. *Gaussian*, 121. Wallingford CT: gaussian. Inc (2009). p. 150–66.
37. De La Torre G, Nicolau M, Torres T. *Phthalocyanines: Synthesis, Supramolecular Organization, and Physical Properties*. *Supramolecular Photosensitive and Electroactive Materials*. Amsterdam(Netherlands): Elsevier (2001). p. 1–111. doi:10.1016/b978-012513904-5/50003-x
38. Rao SV, Krishnakanth KN, Indumathi C, Girisun TS. Non-linear Optical Properties of Novel Nanomaterials. *Handbook Laser Techn Appl Lasers Appl Mater Process Spectrosc* (2021) 3:255. (Volume Three). doi:10.1201/9781315310855-21
39. Banerjee D, Moram SSB, Byram C, Rathod J, Jena T, Podagatlapalli GK, et al. Plasmon-enhanced Ultrafast and Tunable Thermo-Optic Nonlinear Optical Properties of Femtosecond Laser Ablated TiO₂ and Silver-Doped TiO₂ Nanoparticles. *Appl Surf Sci* (2021) 569:151070. doi:10.1016/j.apsusc.2021.151070
40. Sutherland RL. *Handbook of Nonlinear Optics*. Florida(United States): CRC Press (2003).
41. Mushtaq A, Pradhan B, Kushavah D, Zhang Y, Wolf M, Schrenker N, et al. Third-Order Nonlinear Optical Properties and Saturation of Two-Photon Absorption in Lead-Free Double Perovskite Nanocrystals under Femtosecond Excitation. *ACS Photon* (2021) 8(11):3365–74. doi:10.1021/acsphoton.1c01351
42. Hegde PK, Vasudeva Adhikari A, Manjunatha MG, Suchand Sandeep C, Philip R. Novel Poly (3, 4-dialkoxythiophene) S Carrying 1, 3, 4-oxadiazolyl-biphenyl Moieties: Synthesis and Nonlinear Optical Studies. *Polym Int* (2011) 60(1):112–8. doi:10.1002/pi.2919
43. Chen B, Huang X, Gou D, Zeng J, Chen G, Pang M, et al. Rapid Volumetric Imaging with Bessel-Beam Three-Photon Microscopy. *Biomed Opt express* (2018) 9(4):1992–2000. doi:10.1364/boe.9.001992
44. Williams RM, Shear JB, Zipfel WR, Maiti S, Webb WW. Mucosal Mast Cell Secretion Processes Imaged Using Three-Photon Microscopy of 5-hydroxytryptamine Autofluorescence. *Biophysical J* (1999) 76(4):1835–46. doi:10.1016/s0006-3495(99)77343-1
45. Horton NG, Wang K, Kobat D, Clark CG, Wise FW, Schaffer CB, et al. *In Vivo* three-photon Microscopy of Subcortical Structures within an Intact Mouse Brain. *Nat Photon* (2013) 7(3):205–9. doi:10.1038/nphoton.2012.336
46. Moreels I, Hens Z, Kockaert P, Loicq J, Van Thourhout D. Spectroscopy of the Nonlinear Refractive index of Colloidal PbSe Nanocrystals. *Appl Phys Lett* (2006) 89(19):193106. doi:10.1063/1.2385658
47. Ahmed MS, Biswas C, Miranda PB, Raavi SSK. Nonlinear Optical Techniques for Characterization of Organic Electronic and Photonic Devices. *Eur Phys J Spec Top* (2021) 231:1–17. doi:10.1140/epjs/s11734-021-00391-8
48. Venkatram N, Rao DN, Giribabu L, Rao SV. Nonlinear Optical and Optical Limiting Studies of Alkoxy Phthalocyanines in Solutions Studied at 532 Nm with Nanosecond Pulse Excitation. *Appl Phys B* (2008) 91(1):149–56. doi:10.1007/s00340-008-2934-5
49. Ekbote A, Patil P, Mairid SR, Chia TS, Quah CK. Structural, Third-Order Optical Nonlinearities and Figures of merit of (E)-1-(3-substituted Phenyl)-3-(4-Fluorophenyl) Prop-2-En-1-One under CW Regime: New Chalcone Derivatives for Optical Limiting Applications. *Dyes Pigm* (2017) 139:720–9. doi:10.1016/j.dyepig.2017.01.002
50. Biswas C, Krishnakanth K, Lade J, Chaskar A, Tripathi A, Chetti P, et al. Linear and Femtosecond Nonlinear Optical Properties of Soluble Pyrrolo [1, 2-a]

- Quinoxalines. *Chem Phys Lett* (2019) 730:638–42. doi:10.1016/j.cplett.2019.06.062
51. Rao SV, Srinivas NN, Rao DN, Giribabu L, Maiya BG, Philip R, et al. Studies of Third-Order Optical Nonlinearity and Nonlinear Absorption in Tetra Tollyl Porphyrins Using Degenerate Four Wave Mixing and Z-Scan. *Opt Commun* (2000) 182(1-3):255–64. doi:10.1016/s0030-4018(00)00808-7
52. Zadrozna I, Kaczorowska E. Relationship between Structure and Nonlinear Optical Properties of New Bisazo Chromophores. Theoretical and Experimental Study. *Struct Chem* (2008) 19(1):131–5. doi:10.1007/s11224-007-9262-y
53. Iliopoulos K, Czaplicki R, El Ouazzani H, Balandier J-Y, Chas M, Goeb S, et al. Physical Origin of the Third Order Nonlinear Optical Response of Orthogonal Pyrrolo-Tetrathiafulvalene Derivatives. *Appl Phys Lett* (2010) 97(10):101104. doi:10.1063/1.3482943
54. Warde U, Sekar N. NLOphoric Mono-Azo Dyes with Negative Solvatochromism and In-Built ESIPT Unit from Ethyl 1, 3-Dihydroxy-2-Naphthoate: Estimation of Excited State Dipole Moment and pH Study. *Dyes Pigm* (2017) 137:384–94. doi:10.1016/j.dyepig.2016.10.032
55. Prabhakar C, Yesudas K, Bhanuprakash K, Rao VJ, Santosh Kumar RS, Rao DN. Linear and Nonlinear Optical Properties of Mesoionic Oxyallyl Derivatives: Enhanced Non-resonant Third Order Optical Nonlinearity in Croconate Dyes. *J Phys Chem C* (2008) 112(34):13272–80. doi:10.1021/jp803025v
56. Tran K, Scott GW, Funk DJ, Moore DS. Resonantly Enhanced, Degenerate Four-Wave Mixing Measurement of the Cubic Molecular Hyperpolarizability of Squaraine Dyes at 700 Nm. *J Phys Chem* (1996) 100(29):11863–9. doi:10.1021/jp960447n
57. Manzoni V, Modesto-Costa L, Del Nero J, Andrade-Filho T, Gester R. Strong Enhancement of NLO Response of Methyl orange Dyes through Solvent Effects: A Sequential Monte Carlo/DFT Investigation. *Opt Mater* (2019) 94:152–9. doi:10.1016/j.optmat.2019.05.018
58. Sreenath M, Joe IH, Rastogi V. Experimental and Theoretical Investigation of Third-Order Nonlinear Optical Properties of Azo Dye 1-(2, 5-Dimethoxy-Phenylazo)-Naphthalen-2-ol by Z-Scan Technique and Quantum Chemical Computations. *Dyes Pigm* (2018) 157:163–78. doi:10.1016/j.dyepig.2018.04.044
59. Jayarshmi D, Robert HM, Aruldas D. Elucidation of the Structure, Spectroscopic Techniques and Quantum Chemical Investigations on Nonlinear Optical Material 2-Hydroxy-5-Methylbenzaldehyde. *J Mol Struct* (2021) 1238:130426. doi:10.1016/j.molstruc.2021.130426
60. Patil P, Maidur SR, Rao SV, Dharmaparakash S. Crystalline Perfection, Third-Order Nonlinear Optical Properties and Optical Limiting Studies of 3, 4-Dimethoxy-4'-Methoxychalcone Single crystal. *Opt Laser Techn* (2016) 81:70–6. doi:10.1016/j.optlastec.2016.01.033
61. Polavarapu L, Venkatram N, Ji W, Xu Q-H. Optical-limiting Properties of Oleylamine-Capped Gold Nanoparticles for Both Femtosecond and Nanosecond Laser Pulses. *ACS Appl Mater Inter* (2009) 1(10):2298–303. doi:10.1021/am900442u
62. Rao SV, Anusha PT, Prashant TS, Swain D, Tewari SP. Ultrafast Nonlinear Optical and Optical Limiting Properties of Phthalocyanine Thin Films Studied Using Z-Scan. *Mater Sci Appl* (2011) 2(05):299. doi:10.4236/msa.2011.25039
63. Misra N, Rapolu M, Rao SV, Varshney L, Kumar V. Nonlinear Optical Studies of Inorganic Nanoparticles-Polymer Nanocomposite Coatings Fabricated by Electron Beam Curing. *Opt Laser Techn* (2016) 79:24–31. doi:10.1016/j.optlastec.2015.11.004

Conflict of Interest: The authors declare that the research was conducted in the absence of any commercial or financial relationships that could be construed as a potential conflict of interest.

Publisher's Note: All claims expressed in this article are solely those of the authors and do not necessarily represent those of their affiliated organizations, or those of the publisher, the editors, and the reviewers. Any product that may be evaluated in this article, or claim that may be made by its manufacturer, is not guaranteed or endorsed by the publisher.

Copyright © 2022 Ahmed, Biswas, Banerjee, Chetti, Yang, Soma and Raavi. This is an open-access article distributed under the terms of the Creative Commons Attribution License (CC BY). The use, distribution or reproduction in other forums is permitted, provided the original author(s) and the copyright owner(s) are credited and that the original publication in this journal is cited, in accordance with accepted academic practice. No use, distribution or reproduction is permitted which does not comply with these terms.